JOURNAL OF SPACECRAFT AND ROCKETS
Vol. 32, No. 1, January–February 1995

Determination of the Recombination Efficiency of Thermal Control Coatings for Hypersonic Vehicles

R. K. Clark*
NASA Langley Research Center, Hampton, Virginia 23681
G. R. Cunnington Jr.†
Cunnington Associates, Palo Alto, California 94306
and
K. E. Wiedemann‡
Analytical Services and Materials, Inc., Hampton, Virginia 23665

A method is presented for determining the recombination efficiency of coatings for hypersonic vehicle applications. The approach uses experimental results from arc-jet tests with an analysis to determine the efficiency for the recombination of atomic species present in the boundary layer. The analysis employs analytical solutions to the laminar boundary-layer heat-transfer equations with experimental heating-rate, temperature, and pressure measurements. The authors discuss experimental difficulties in achieving reliable materials-performance data. The utility of the method is that it provides a rapid and efficient tool for use in qualitative screening and development of materials. The effects of second-order heat-transfer terms may be as high as 50% for low-catalysis surfaces. With the second-order terms included, the maximum uncertainty in recombination-efficiency data for low-catalysis surfaces is 45%. The discussions are based on experimental data and calculations for arc-jet tests of the titanium alloy Ti-14Al-21Nb with a borosilicate-like glass coating that has a recombination efficiency of about 0.006 to 0.01.

Nomenclature

C = specific heat
c_e = freestream atomic mass fraction
d = sample diameter, m
d_{eff} = effective nose diameter of sample, m
$e_b(\lambda, T)$ = spectral emissive power of a blackbody at temperature T and wavelength λ, W/m^2
F_e = radiation heat-transfer factor for sample edge
F_h = radiation heat-transfer factor for insulator hole
h_{bse} = stagnation stream frozen enthalpy, J/kg
h_{rN_2} = heat of recombination of nitrogen, J/kg
h_{rO_2} = heat of recombination of oxygen, J/kg
h_{rse} = stagnation stream recombination enthalpy, J/kg
h_{se} = stagnation stream total enthalpy, J/kg
K_{air} = constant in equation for h_{se}, kg/m$^{\frac{3}{2}}$-s-Pa$^{\frac{1}{2}}$, Eq. (25)
k_{ins} = thermal conductivity of the insulation layer, W/m-K
k_w = catalytic reaction rate constant, m/s
L_e = Lewis number, 1.4
l = thickness, m
l_g = width of gap between sample and model adapter, m
M_A = atomic weight of dissociated air, kg/mole
P = pressure, Pa
Pr = Prandtl number, 0.72
q = heat-transfer rate, W/m^2
q_D = heat transfer by diffusion, W/m^2
q_{diff} = iteration parameter, Eq. (27)
R_u = Universal gas constant, J/mole-K
S = boundary-layer diffusion rate, m/s
T = temperature, K
T_b = temperature at the back of the insulation layer, K
T_{eq} = radiation equilibrium temperature, K
T_0 = initial sample temperature, K
U = velocity of gas, m/s
β = velocity gradient in boundary layer, s^{-1}
γ = recombination efficiency of sample
ΔT = difference between sample temperature and model adapter temperature, K
$\Delta\lambda$ = wavelength interval, m
$\partial T/\partial t$ = temperature rise rate of the sample, K/s
ε = emittance of sample
$\varepsilon(\lambda)$ = room-temperature spectral near-normal emittance at wavelength λ
λ = wavelength, m
μ = viscosity of test gas, Pa/s
ρ = density of test gas, kg/m^3
σ = Stefan-Boltzmann constant, W/m^2-K^4
ϕ = recombination factor

Subscripts

absorp = absorption by sample
aero = aerothermal
arc = arc chamber
c = convection
cat = catalytic
ccw = catalytic cold-wall
cond = conduction
ec = edge conduction
hc = hole conduction
ins = insulator
nom = no second-order heat-transfer terms
rad = radiative
s = sample
se = stream stagnation condition
TN = total normal
t/c = thermocouple
TH = total hemispherical
w = sample wall condition
∞ = freestream condition

Superscript

t = transient condition

Received April 18, 1994; revision received July 18, 1994; accepted for publication Aug. 9, 1994.

*Senior Research Engineer. Member AIAA.
†President.
‡Senior Scientist.

Introduction

FOR flight conditions involving nonequilibrium chemistry with dissociated species, the convective heat transfer to a vehicle consists of a conduction component plus a diffusion component that is due to recombination at the vehicle surface of the dissociated gas species. The catalytic effects of the vehicle surface govern the magnitude of the diffusion component of the heat transfer. The diffusion component of the heat transfer may be greater than the conduction heat transfer. The parameter called recombination efficiency provides a means for scaling the catalytic effects of the surface and the resultant diffusional heat transfer. Figure 1 shows heat-transfer rate results for a sample exposed to an arc-jet environment in stagnation flow at a freestream Mach number of 4, a boundary-layer edge enthalpy of 8.1 MJ/kg, and a wall pressure of 786 Pa. The conduction heat-transfer rate is about 120 kW/m^2, and the total heat-transfer rate for a recombination efficiency of unity is 320 kW/m^2. The total convection heat-transfer rate for a recombination efficiency of 0.01 is about 140 kW/m^2. These very substantial differences in heat transfer may translate to large differences in the surface temperature of flight vehicles.

Current materials of interest for the hot structure and heat shield of hypersonic vehicles require environmental and thermal control coatings to expand their range of application. Protective thermal-control coatings that shield materials from oxidation enable their use at higher temperatures. Additionally, coatings that provide a high-emittance and low-catalysis surface extend the applicability of materials by reducing the net rate of heat transfer to vehicles in hypersonic flight.[1] In a nonequilibrium flow, low-catalysis surfaces result in low efficiency for wall recombination of dissociated species with an attendant reduction in diffusional heat-transfer rate. Also, high-emittance surfaces reject a significant portion of the absorbed heat by reradiation.

Accurate data for recombination efficiency are particularly critical in the design of minimum-weight metallic structures because of the strong temperature dependence of oxidation and mechanical properties of superalloys and high-strength-to-weight materials (like titanium and titanium-aluminide intermetallic alloys) near their maximum use temperatures. Therefore, a critical part of developing materials and coatings for hypersonic vehicle applications involves conducting meaningful ground tests of coated samples to obtain surface recombination-efficiency data.

A stagnation laminar boundary-layer heat-transfer method[2,3] permits calculating the rate of heat transfer to bodies of known recombination efficiency in hypersonic dissociated flows. Conversely, the stagnation laminar boundary-layer heat-transfer method with heat-transfer measurements and an energy balance on samples permits calculating their recombination efficiency.[4] These approaches provide the basis for developing an efficient low-cost procedure for evaluating the recombination efficiency of samples using experimental data from hypersonic flow tests.

This paper presents experimental and analytical techniques that enable determination of the recombination efficiency of coatings for hypersonic vehicle applications. The techniques use heat-transfer calculations with a detailed energy balance. These data are used in a computer solution of the stagnation boundary-layer equations to obtain qualitative data for recombination efficiency of coating surfaces at different operating conditions. Samples were exposed to dynamic oxidation conditions in an electric-arc-heated hypersonic wind tunnel. This paper addresses problems and uncertainties encountered in conducting experimental evaluations of low-catalysis coatings for hypersonic vehicles. The utility of the method is that it provides a rapid and efficient tool for use in screening and development of materials.

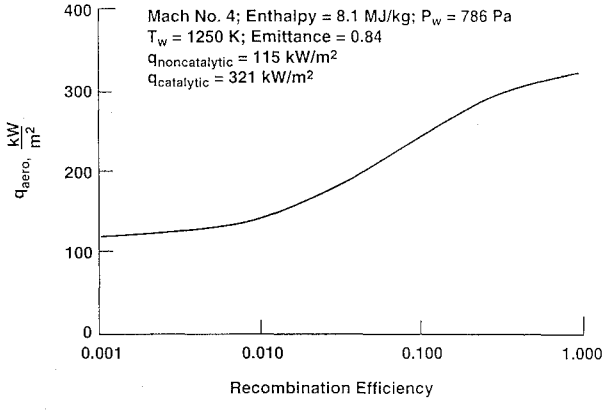

Fig. 1 Variation in aerothermal heating with recombination efficiency for arc-jet environment.

Experimental Method

Exposure to Simulated Hypersonic Flow

Material samples are tested, under dynamic oxidation conditions similar to hypersonic flight, in the NASA Langley Research Center Hypersonic Materials Environmental Test System (HYMETS), an electric-arc-heated hypersonic wind tunnel that provides for efficient testing of material samples under dynamic oxidation conditions.[5] The HYMETS is a 100-kW constrictor-arc-heated wind tunnel that uses air plus nitrogen and oxygen gases in ratios equivalent to air. In the HYMETS, gases enter the arc chamber containing a direct-current arc, reach a very high energy level, and expand through a supersonic nozzle into the test chamber, which is under vacuum. The hypersonic flow impinges on the test sample mounted in a stagnation configuration and exhausts through a mechanically pumped diffuser system.

Table 1 shows the range of test conditions available in the HYMETS. These conditions do not fully simulate hypersonic flight. However, heating of the sample with high-velocity air is critical to evaluating the response of materials and surfaces to hypersonic flight. The range of heat transfer possible in the HYMETS includes the levels encountered by a significant portion of a vehicle in hypersonic flight. Chemical equilibrium calculations for the range of test conditions of the present study indicate that more than 95% of the oxygen in the test stream is atomic and less than 5% of the nitrogen is atomic.[1]

The HYMETS contains three water-cooled air-actuated struts that facilitate exposure of samples and instrumentation to the test environment. Figure 2 shows the sample-model adapter used to fasten samples to the strut. The sample-model configuration consists of a 2.5-cm-diam sample disk mounted to a 3.3-cm-diam copper model holder that attaches to a water-cooled strut. The sample is instrumented with a Pt/Pt13%Rh thermocouple. The 0.25-mm-diam

Table 1 Range of operating conditions for HYMETS facility

Parameter	Range
Mach number	3.5–4.4
Wall pressure, Pa	525–850
Stream enthalpy, MJ/kg	3.5–10.0
Catalytic cold-wall heating rate, kW/m^2	60–425
Equilibrium dissociation, %:	
Oxygen	0–100
Nitrogen	≤5

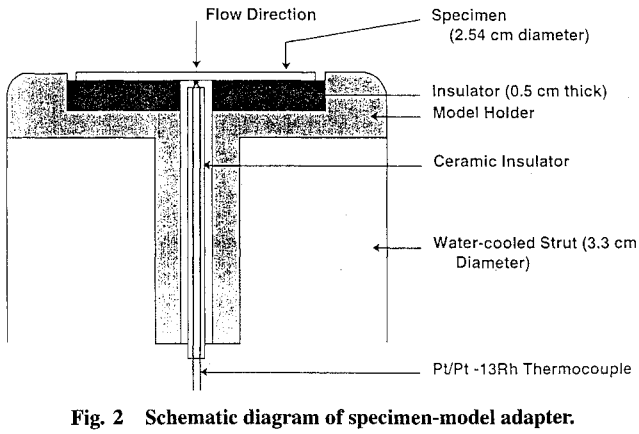

Fig. 2 Schematic diagram of specimen-model adapter.

thermocouple wire is contained in a 0.8-mm-diam alumina tube. The sample is insulated from the model holder by a 6-mm-thick fibrous silica insulator. The thermocouple assembly passes through a 3.18-mm-diam hole in the insulator and the model adapter.

A combined water-cooled heat-transfer and pressure probe, which has the same geometry as the sample-model adapter and mounts on a different insertion sting, is used to measure the catalytic cold-wall heat-transfer rate and the surface pressure. The heat-transfer sensor of the probe is a circular foil heat-flux gauge made of constantan.[6] The water-cooled heat-transfer probe is calibrated against a silver slug calorimeter of the same geometry as the sample-model adapter. Silver is the preferred material for reference, because it has a high recombination efficiency for oxygen ($\gamma = 0.25$).[7] Upon exposure of the silver sample to the heating environment, its temperature is low, and the resultant heating of the sample is the catalytic cold-wall heat-transfer rate (q_{ccw}).

Test conditions are continuously monitored from the start of a HYMETS test. At the start of a test, the sample temperature is transient and, because the heat loss by radiation is negligible at low temperature, incoming heat is accommodated by increasing the temperature of the sample and by conduction to the sample-model adapter. After some time, the sample reaches the radiation equilibrium temperature for the test condition, and the heat-transfer rate to the sample equals the heat losses due to radiation and conduction to the sample-model adapter. Parameters measured during a test include the temperature and composition of gases injected into the arc chamber, arc-chamber pressure, test-chamber pressure, pressure at the sample surface, sample temperature, and catalytic cold-wall heat-transfer rate (q_{ccw}).

Characterization of Radiative Properties

Room-temperature spectral near-normal reflectance measurements are made over the wavelength range from 1.5 to 25 μm using a heated cavity reflectometer.[8] The spectral emittance is obtained from the reflectance using the relationships that absorptance equals unity minus reflectance and (from Kirchhoff's law) spectral emittance equals spectral absorptance. The total emittance is calculated from the spectral emittance using the equation[9]

$$\varepsilon_{TN} = \frac{\sum \varepsilon(\lambda, T) e_b(\lambda, T)\, \Delta\lambda}{\sum e_b(\lambda, T)\, \Delta\lambda} \tag{1}$$

These are total-normal-emittance data: heat-transfer analyses require total-hemispherical-emittance data (ε_{TH}). The latter are obtained from the equation[10,11]

$$\varepsilon_{TH} = 0.975\varepsilon_{TN} \tag{2}$$

Materials and Coatings

For testing, the low-catalysis coatings were applied to a substrate of Alpha-2 titanium-aluminide intermetallic alloy. The alloy has a nominal weight percentage composition of 14 aluminum, 21 niobium, and the balance titanium, and a density of 4.6 g/cm^3. The low-catalysis coating is a borosilicate-like glass prepared by physical vapor deposition and chemical vapor deposition. Reference 12 describes the processing of this coating, which is about 5 μm thick, and other similar low-catalysis coatings.

Analysis

References 2, 13, and 14 treat aerothermal heat transfer to hypersonic flight vehicles. The heat transfer to a body in hypersonic flow (q_{aero}) consists of a conduction component (q_c) and a diffusion component (q_{cat}):

$$q_{aero} = q_c + q_{cat} \tag{3}$$

The conduction heat transfer results from transport of thermal energy to the vehicle surface through a temperature gradient. The diffusion component results from the transport of energy due to a species gradient and surface catalytic properties that affect the recombination of dissociated species.

The approach of Goulard for computing catalytic heating[2] is applied to the stagnation-point laminar-boundary-layer heat-transfer technique of Fay and Riddell[14]:

$$q_c = 0.763 Pr^{-0.6}\left(\frac{\mu_w \rho_w}{\mu_{se}\rho_{se}}\right)^{0.1} (\beta \mu_{se}\rho_{se})^{0.5}\left(\frac{h_{se} - h_w}{h_{se}}\right) h_{bse} \tag{4}$$

$$q_{cat} = q_D \phi \tag{5}$$

where

$$h_{bse} = h_{se} - h_{rse} \tag{6}$$

$$h_{rse} = h_{rO_2} c_e \qquad \text{(for oxygen atoms only)} \tag{7}$$

$$h_{rse} = 0.2346 h_{rO_2} + h_{rN_2}(c_e - 0.2346) \quad \text{(for oxygen and nitrogen atoms)} \tag{8}$$

$$q_D = 0.763 Pr^{-0.6} L_e^{0.63}\left(\frac{\mu_w \rho_w}{\mu_{se}\rho_{se}}\right)^{0.1} \times (\beta \mu_{se}\rho_{se})^{0.5}\left(\frac{h_{se} - h_w}{h_{se}}\right) h_{rse} \tag{9}$$

$$\beta = 2\frac{U_\infty}{d_{eff}}\left[\frac{\rho_\infty}{\rho_{se}}\left(2 - \frac{\rho_\infty}{\rho_{se}}\right)\right]^{0.5} \tag{10}$$

$$\phi = \frac{1}{1 + S/k_w} \tag{11}$$

$$S = 0.763 \frac{Pr^{-0.6} L_e^{0.63}}{\rho_w}\left(\frac{\mu_w \rho_w}{\mu_{se}\rho_{se}}\right)^{0.1} (\beta \mu_{se}\rho_{se})^{0.5} \tag{12}$$

and

$$k_w = \gamma\left(\frac{R_u T_w}{2\pi M_A}\right)^{0.5} \tag{13}$$

The effective diameter of the sample, d_{eff}, in Eq. (10) is defined by[15]

$$d_{eff} = 3.78d \tag{14}$$

The factor ϕ accounts for the recombination rate of atoms diffusing to the surface. This model assumes that the total heat of recombination for the atoms reacting at the surface transfers to the surface.

The aerothermal heat transfer balances the heat absorption and losses by the sample. In a one-dimensional surface energy balance the aerothermal heat-transfer rate (q_{aero}) equals the sum of heat absorption (q_{absorp}), heat rejection by radiation (q_{rad}), and heat lost by conduction (q_{cond}):

$$q_{aero} = q_{absorp} + q_{rad} + q_{cond} \tag{15}$$

where

$$q_{absorp} = \rho_s C_s l_s \frac{\partial T_s}{\partial t} \tag{16}$$

$$q_{rad} = \varepsilon_{TH} \sigma T_s^4 \tag{17}$$

$$q_{cond} = 2\left[\frac{\rho_{ins} C_{ins} k_{ins}}{\pi}(T_s - T_0)\frac{\partial T_s}{\partial t}\right]^{0.5} \tag{18}$$

for transient heating, and

$$q_{cond} = k_{ins}\frac{T_s - T_b}{l_{ins}} \tag{19}$$

for thermal equilibrium heating. Equation (18) is the solution to the semi-infinite conduction problem.

At the outset of exposure, the temperature of a body subjected to aerothermal heating is transient and, because the temperature is initially low, heat rejection by radiation is negligible. Thus for

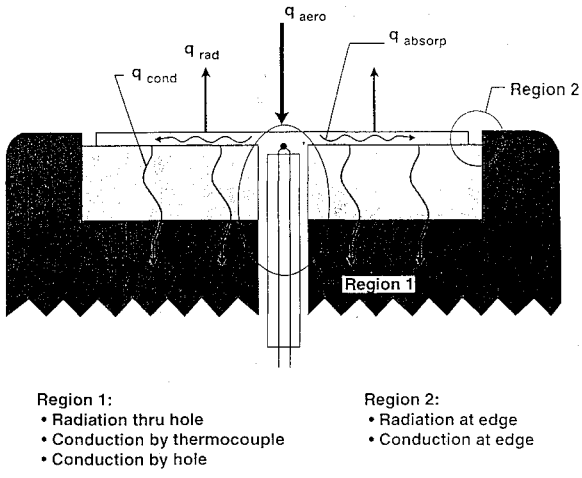

Fig. 3 Energy-balance diagram for sample-model adapter.

transient-heating conditions, the aerothermal heat-transfer rate is given by

$$q_{\text{aero}} = \rho_s C_s l_s \frac{\partial T_s}{\partial t} + 2\left[\frac{\rho_{\text{ins}} C_{\text{ins}} k_{\text{ins}}}{\pi}(T_s - T_0)\frac{\partial T_s}{\partial t}\right]^{0.5} \tag{20}$$

Equation (20), applied to the silver sample used to calibrate the heat-transfer probe, yields the cold-wall heat transfer rate to a catalytic surface (q_{ccw} for $\gamma = 0.25$). After some time, when the sample temperature has stabilized, thermal equilibrium conditions exist, and heat absorption defined by Eq. (16) is negligible, the radiation equilibrium heat-transfer rate is given by

$$q_{\text{aero}} = \varepsilon_{\text{TH}} \sigma T_s^4 + k_{\text{ins}}\left(\frac{T_s - T_b}{l_{\text{ins}}}\right) \tag{21}$$

Catalysis calculations for the transient portion of the test determine the cold-wall recombination efficiency, and for the thermal-equilibrium portion of the test determine the hot-wall recombination efficiency at test temperature. However, a simple one-dimensional surface energy balance is not adequate to describe the heat transfer to a model undergoing aerothermal heating in an electric-arc-heated wind tunnel. Figure 3 shows an energy balance diagram for the sample-model adapter assembly. The two regions labeled in the figure involve second-order heat-transfer processes that must be evaluated to improve the accuracy of the analysis, particularly for materials having low recombination efficiencies. Region 1, where the back-surface thermocouple passes through the insulation layer, is the site of heat transfer by conduction along the thermocouple and insulator, by conduction through the gas, and by radiation through the hole. Region 2, the gap between the sample edge and the model adapter, is the site of radiative heat transfer between the edge surface, the exposed surface of the insulator, the inner surface of the model adapter, and the test chamber, and of conductive heat transfer between the edge surface and the surrounding gases.

In view of this discussion, Eqs. (20) and (21) must be adjusted to allow for second-order heat-transfer effects. Thus, for transient-heating conditions, Eq. (20) becomes

$$q_{\text{aero}} = \rho_s C_s l_s \frac{\partial T_s}{\partial t} + 2\left[\frac{\rho_{\text{ins}} C_{\text{ins}} k_{\text{ins}}}{\pi}(T_s - T_0)\frac{\partial T_s}{\partial t}\right]^{0.5} + q'_{\text{ec}} + q'_{\text{t/c}} \tag{22}$$

where the factors q'_{ec} and $q'_{\text{t/c}}$ take account of conduction heat transfer at the edge and along the thermocouple and insulator, respectively. The edge-conduction correction is analyzed in terms of a gap width l_g and the temperature difference between the sample and the model holder, $\Delta T'$. In estimating this term, the pressure of air in the gap is the measured sample wall pressure, and the rise in temperature of the model holder is neglected (the copper model holder is taken to be an infinite sink). For these conditions, the edge-conduction correction at a sample temperature of 325 K (the temperature corresponding to $\partial T/\partial t$) is estimated to be $0.375 l_s$.

Table 2 Heat loss correction factor F_e for specimen edge radiation loss as a function of specimen thickness and emittance for model holder emittance of 0.85 and $T = T_s - 100$

Specimen thickness, cm	F_e		
	$\varepsilon = 0.6$[a]	0.80	0.90
0.045	0.0368	0.0361	0.0356
0.065	0.0498	0.0483	0.0476
0.075	0.0565	0.0546	0.0537
0.095	0.0667	0.0642	0.0630

[a]Specimen emittance.

Table 3 Heat-loss correction factor F_h for radiation heat loss through the insulator hole

Specimen temperature, K	F_h			
	$\varepsilon = 0.75$[a]	0.8	0.85	0.9
1100	0.0085	0.0089	0.0092	0.0095
1200	0.0103	0.0106	0.0108	0.0111
1300	0.0116	0.0118	0.0119	0.0121

[a]Specimen emittance.

To calculate heat conduction along the thermocouple-insulator assembly for low-temperature transient conditions, heat loss from the thermocouple wire surfaces is neglected and the problem reduces to the semi-infinite heat-transfer problem, whose solution for the insulation layer is represented by Eq. (18). The ratio of heat conduction along the thermocouple to heat conduction to the insulator is 0.0215. Thus the q_{cond} term multiplied by the factor 1.0215 includes the $q'_{\text{t/c}}$ term, and Eq. (20) becomes

$$q_{\text{aero}} = \rho_s C_s l_s \frac{\partial T_s}{\partial t} + 2.043\left[\frac{\rho_{\text{ins}} C_{\text{ins}} k_{\text{ins}}}{\pi}(T_s - T_0)\frac{\partial T_s}{\partial t}\right]^{0.5} + 0.375 l_s \tag{23}$$

For thermal equilibrium conditions, Eq. (21) becomes

$$q_{\text{aero}} = \varepsilon_{\text{TH}} \sigma T_s^4 (1 + F_e + F_h) + k_{\text{ins}}\left(\frac{T_s - T_b}{l_{\text{ins}}}\right) + q_{\text{ec}} + q_{\text{hc}} + q_{\text{t/c}} \tag{24}$$

where the factors F_e and F_h take account of radiation heat transfer at the sample edge and through the hole, respectively, and the terms q_{ec}, q_{hc}, and $q_{\text{t/c}}$ take account of conduction heat transfer at the edge and conduction through the insulator hole and along the thermocouple-insulator assembly, respectively.

The edge-radiation correction factor F_e is based upon the radiosity of the sample edge, model adapter, insulator surface, and test chamber. Assumptions invoked in estimating the factor are the following: all surfaces are gray and diffuse, the emittance of the sample edge is the same as that of its top surface, and the sample and insulator are at the same temperature. Table 2 presents data for F_e as a function of sample thickness and emittance values of 0.6, 0.8, and 0.9. The data are for an insulator reflectance of 0.50, a model adapter emittance of 0.85, and a model adapter temperature 100 K lower than the sample temperature.

The hole radiation correction factor F_h is similarly based upon the radiosity of the sample and the insulator hole. The mean insulator temperature used to calculate the radiosity of the hole was estimated, from experimental measurements of the temperature gradient across the insulator, to be 100 K lower than the sample temperature. Table 3 presents data for F_h as a function of sample emittance and temperature.

The terms q_{ec}, q_{hc}, and $q_{\text{t/c}}$ are presented as a function of temperature in Table 4. The edge conduction correction is expressed in terms of gap width l_g and the temperature difference between the sample and the model holder, ΔT. In estimating this term, the pressure of air in the gap is taken to be the same as the measured sample wall pressure, and the Knudsen number is based on the gap width. The heat conduction through the hole in the insulator is estimated using the conductivity of air at the average temperature of the

Table 4 Second-order heat transfer terms[a]

Temperature, K	$q_{ec}/(l_g \Delta T)$,[b] kW/m^3-K	q_{hc},[c] kW/m^2	$q_{t/c}$,[d] kW/m^2
1100	18.200	0.314	2.469
1200	19.414	0.523	2.803
1300	20.836	0.782	3.180

[a]For Eq. (23).
[b]Heat-loss parameter for conduction heat transfer from sample edge as a function of sample temperature.
[c]Heat loss through insulator hole as a function of the average insulator temperature.
[d]Conduction heat loss to thermocouple and insulator as a function of sample temperature.

insulator. The average temperature of the insulator was determined experimentally to be about 100 K lower than the sample temperature. The rate of heat conduction along the thermocouple-insulator assembly was calculated by assuming a circular fin with two discrete temperature zones: one corresponding to the thickness of the insulator and the second contained within the model adapter. The latter is assumed to be at 300 K. In each case heat transfer from the surface of the assembly is by radiation.

Computation Procedure

Results from the energy balance are used with the Fay-Riddell method for stagnation-point laminar-boundary-layer heat transfer, including the modification of Goulard for recombination rates, to determine the recombination efficiency of samples. Assumptions invoked in performing the analysis are: the solution to the stagnation boundary-layer equations is valid; the total flow process is isentropic; the test gas is in chemical equilibrium in the arc chamber, in the free stream, and at the boundary-layer edge; and the test-gas chemistry is frozen in the boundary layer. This last assumption is restrictive, but is necessary in order to create a compact and efficient analysis suitable for use with a personal computer.

Measurements made during a HYMETS test of a sample together with results from the surface energy balance define the sample heat-transfer rate, temperature, pressure, and emittance; the catalytic cold-wall heat-transfer rate; the freestream pressure; and the arc-chamber pressure. The recombination efficiency of the heat-transfer probe is known from the literature.[7] Steps in the computation procedure are as follows:

1) Calculate the boundary-layer edge enthalpy using the result of Zoby and Sullivan[16] with the catalytic cold-wall heat-transfer rate measured with the heat-transfer probe:

$$h_{se} = \frac{q_{ccw}}{K_{air}} \left(\frac{d_{eff}}{2P_w} \right)^{0.5} - h_w \tag{25}$$

where d_{eff} for a flat-face disk is given by Eq. (14), and

$$K_{air} = 0.000388 \frac{kg}{m^{\frac{3}{2}} - s - P_w^{\frac{1}{2}}} \tag{26}$$

2) Use the chemical equilibrium analysis of Stroud and Brinkley[17] with the isentropic relationships, the stream stagnation enthalpy, and the pressures at the wall, in the arc chamber, and in the freestream to calculate the temperature, enthalpy, and composition in those regions.

3) Use the viscosity power-law approximation for the viscosity of air with an exponent of $\frac{2}{3}$ to determine its value at the wall and in the freestream.[18]

4) Use the gas law with compressibility factor to determine the gas density at the wall, in the freestream, and at the boundary-layer edge.

5) Adjust the boundary-layer edge enthalpy so that the calculated heat-transfer rate obtained from Eqs. (3–14) (for $\gamma = 0.25$ and $T_w = 300$ K) equals the value determined with the heat-transfer probe:

$$q_{diff} = 1 - \frac{q_c - q_D \phi}{q_{ccw}} \tag{27}$$

Iterate through steps 2–5 until $q_{diff} \leq 0.00001$.

6) Calculate the rate of heat transfer to the sample using Eq. (23) or (24).

7) Calculate S, q_c, and q_D for h_{se}, P_w, and T_w.

8) Calculate ϕ using the results from steps 6 and 7 above:

$$\phi = \frac{q_{aero} - q_c}{q_D} \tag{28}$$

9) Calculate k_w and γ using Eqs. (11) and (13):

$$k_w = -\frac{S}{1 - 1/\phi} \tag{29}$$

$$\gamma = k_w \left(\frac{2\pi M_A}{R_u T_w} \right)^{0.5} \tag{30}$$

Catalysis calculations for the transient portion of the test determine the cold-wall recombination efficiency, and for the steady-state portion of the test determine the hot-wall recombination efficiency at the test temperature.

Results and Discussion

The experimental parameters required as inputs to the analysis for determining the recombination efficiency are the temperature or temperature rise rate and emittance of the sample; the pressure at the sample surface, in the freestream of the flowfield, and in the arc chamber of the arc jet; and the catalytic cold-wall heat-transfer rate. Uncertainty in measurement of any of these parameters affects the confidence level of the calculated results. Figure 4 shows results from a sensitivity analysis of these parameters for a low-catalysis coating under transient heating conditions. Comparable results for steady-state conditions are shown in Fig. 5. Results for each parameter were obtained by perturbing it while the values used for the remaining parameters were their nominal values. The data show that recombination efficiency is not highly sensitive to deviations in any of the pressure parameters. Deviations in sample temperature or temperature rise rate have the most profound impact on computed results for the recombination efficiency.

Figure 6 shows a comparison of the second-order heat-loss terms with the nominal aerothermal heat-transfer rate for a low-catalysis coating tested at 1250 K. The largest of the second-order terms is the radiation-loss term for the edge, which is about 5% of the nominal aerothermal heat transfer. All the second-order terms sum to about 11% of the nominal aerothermal heat transfer.

Figure 7 shows a comparison of hot-wall recombination-efficiency results obtained with the nominal energy balance and with the energy balance including the second-order terms. These results are for a coating with a very low recombination efficiency. If the second-order terms are included in the analysis, the calculated recombination efficiency increases by about one-half. At low recombination efficiencies, the slope of the curve in Fig. 1 is quite low, so that a small change in aerothermal heating results in a large change in recombination efficiency.

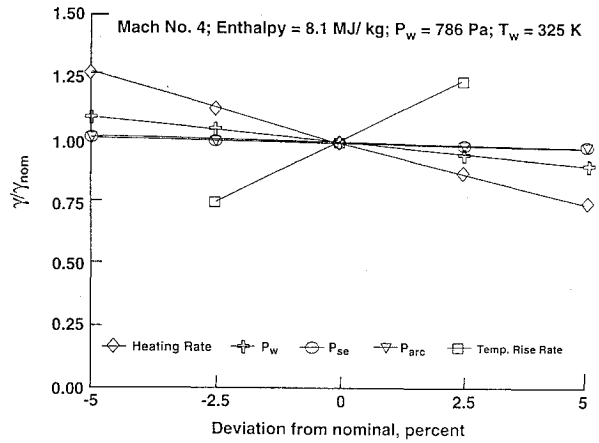

Fig. 4 Sensitivity analysis for low-catalysis coating under cold-wall conditions (325 K).

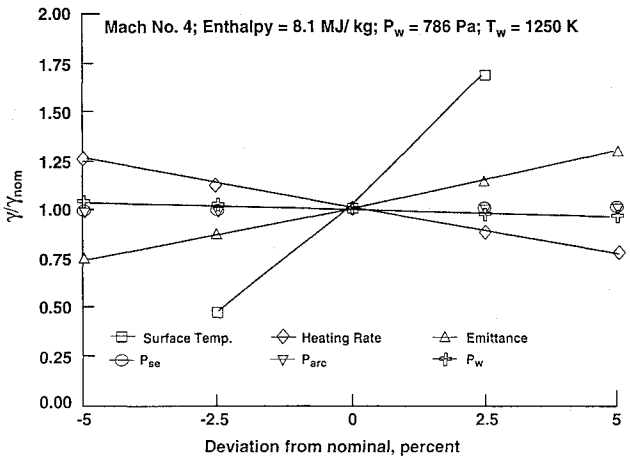

Fig. 5 Sensitivity analysis for low-catalysis coating under hot-wall conditions (1250 K).

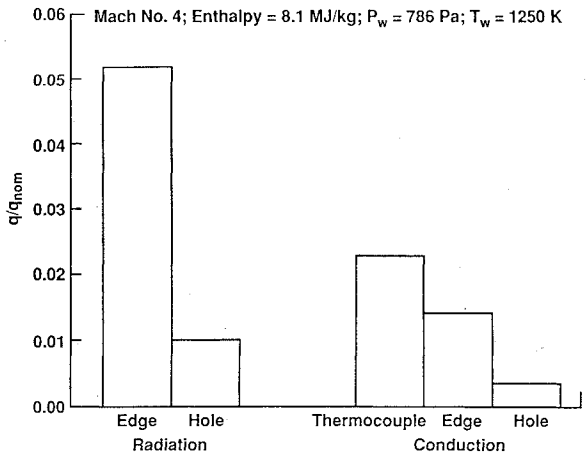

Fig. 6 Comparison of second-order heat-transfer terms.

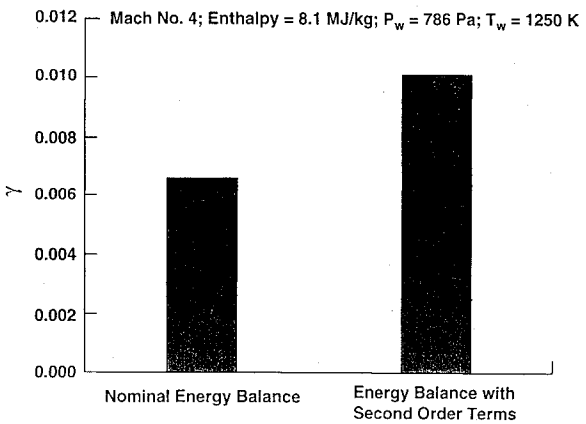

Fig. 7 Effect of second-order heat-transfer terms on recombination efficiency of low-catalysis coating.

The accuracy of the recombination-efficiency results derived by the present technique hinges directly on the assumptions invoked in the analysis and on the uncertainties in experimental test parameters. One major assumption is that chemical equilibrium exists for the test gases in the arc chamber, in the freestream, and at the boundary-layer edge and that frozen chemistry exists in the boundary layer. The thermodynamic state of the test gases in the HYMETS facility is not known; however, it is almost certain that they are not in chemical equilibrium, and there are probably ionized species present. However, because the treatment of reacting flows is beyond the scope of this analysis, the assumption of chemical equilibrium was necessary to get an initial estimate of the reacting-flow problem. At

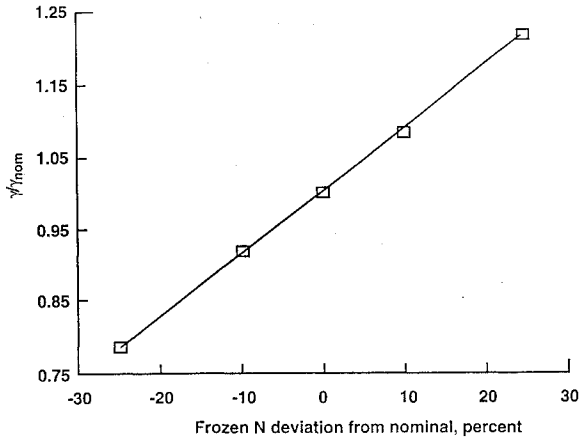

Fig. 8 Effect of uncertainty in atomic-nitrogen fraction on recombination efficiency.

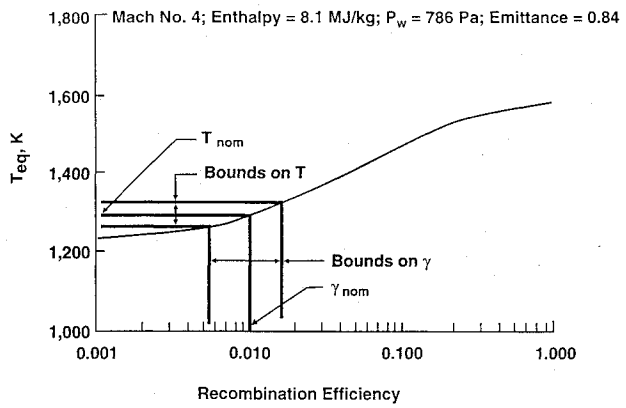

Fig. 9 Variation in radiation equilibrium wall temperature with recombination efficiency.

the outset, the analysis with the assumption of chemical equilibrium was yielding negative values for recombination efficiency of very low-catalysis materials. Hence, a further stipulation regarding chemistry of the test gases was mandated: a fraction of nitrogen is frozen in the atomic state. The atom fraction of nitrogen present was stipulated to vary linearly with the rate of cold-wall catalytic heat transfer from about 0.15 at very low rates of heat transfer to about 0.20 at very high rates. Figure 8 shows that recombination efficiency is not a strong function of the fraction of atomic nitrogen.

Figures 4 and 5 show the effect of uncertainties in test parameters on results of the current analysis and experiment. The most sensitive parameter is the sample surface temperature or temperature rise rate, followed by the catalytic cold-wall heat transfer rate, surface emittance, and pressures in order of decreasing importance. Estimates of maximum uncertainties in measurements of sample temperature or temperature rise rate, heat transfer rate, and emittance are 0.5, 5, and 2.5%, respectively. The estimated accuracy of pressure measurements is greater than 95%. The maximum uncertainty in recombination efficiency based upon the individual maximum uncertainties is about 45%, for a nominal recombination efficiency of 0.010, the bounds would be 0.006 and 0.015.

The contributions of uncertainties in the terms for conduction heat transfer through the insulator and in the second-order heat-transfer terms to recombination efficiency are small. Assuming a 25% maximum uncertainty for each, the maximum uncertainty in recombination efficiency is about 0.002 (20%) for nominal recombination efficiencies near 0.010.

Interest in recombination efficiency relates to its effect on the vehicle heat-transfer rate in hypersonic flight and the resultant temperatures encountered by the vehicle structure. Figure 9 shows the variation in radiation equilibrium wall temperature with recombination efficiency for arc-jet tests of samples exposed to stagnation flow at a freestream Mach number of 4, a freestream enthalpy of

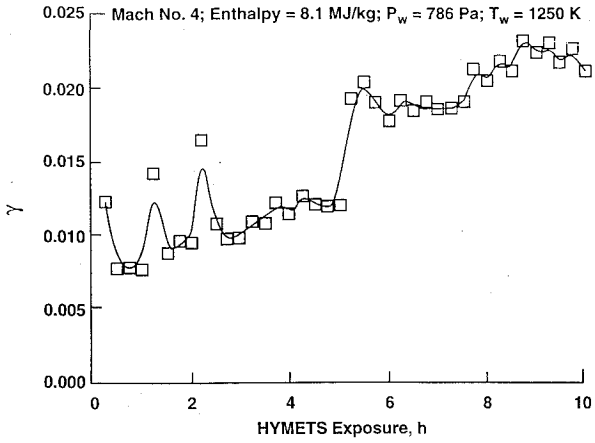

Fig. 10 Variation in hot-wall recombination efficiency of a low-catalysis coating with time of exposure to dynamic oxidation conditions in the HYMETS facility.

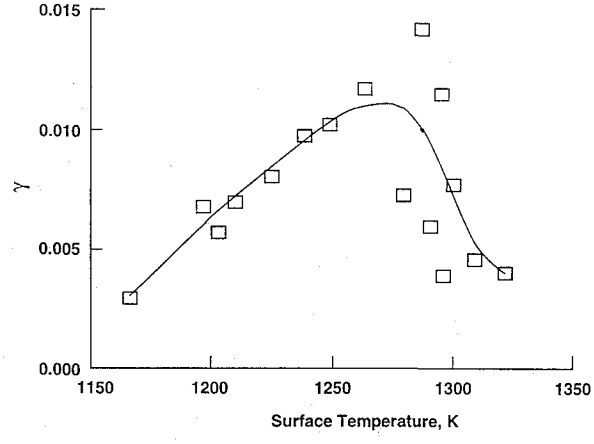

Fig. 11 Variation in recombination efficiency of low-catalysis coating with exposure temperature.

8.1 MJ/kg, and a wall pressure of 786 Pa. For nonequilibrium flow conditions, there is a potential for a tremendous payoff in reduction of temperature from using low-catalysis coatings on vehicle surfaces. For the results presented earlier, a sample whose recombination efficiency is 0.010 (±45%), under dynamic oxidation exposure in an arc-jet, the bounds on the radiation equilibrium wall temperature are 1260 and 1310 K.

Most materials exposed to dynamic oxidation conditions experience some interaction with the high-energy environment. Low-catalysis coatings designed for use under those conditions also undergo change with time of exposure. Figure 10 shows the variation in recombination efficiency of a low-catalysis coating with time of exposure. The reason for the three spikes at times of $\frac{1}{4}$, 1, and 2 h and the shift at 5 h are not known. It is possible the spikes are the result of contamination of the sample by moisture during measurements of radiative properties made at those times. The shift in recombination efficiency at 5 h may relate to some physical-chemical change in the coating that occurs with long-term exposure.

The dissociation and recombination reactions of atomic species are temperature-sensitive phenomena. Figure 11 shows data for recombination efficiency of a low-catalysis coating at temperatures of 1167 to 1322 K. The recombination-efficiency data range from about 0.003 to 0.014. The increase in recombination efficiency with temperature to some level, followed by a decrease, has been documented.[4,19,20] It is probable that the wide range in the data above 1265 K is reflective of instability of the coating and relates to changes occurring in the coating such as increased loss of boron and softening at the higher temperatures. The oscillatory behavior indicated in Fig. 11 is not real, but indicates the range in data for the coating as it experiences thermal-chemical changes. The peak in recombination efficiency at 1290 K is lower than Kolodziej and Stewart[19] observed in their tests of a similar coating. The coating

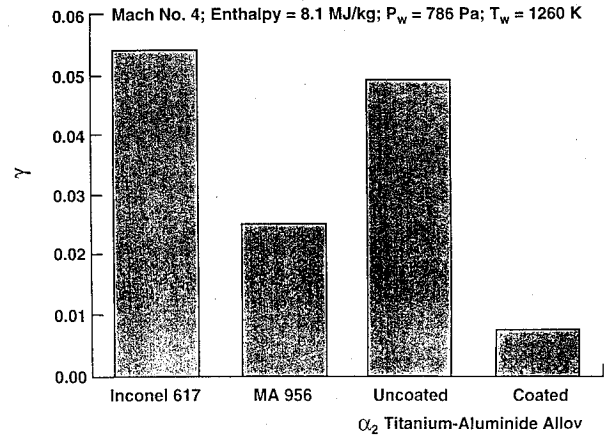

Fig. 12 Comparison of recombination efficiency of low-catalysis coating and uncoated alloys.

tested in this study and the coating reported in Ref. 19 were borosilicate glass; however, their chemistry differences are probably large enough to cause a shift in the location of the peak recombination efficiency.

The range of recombination efficiencies encountered with metals varies with their surface condition. Metals exposed to a high-energy environment undergo oxidation, forming metal oxides, which generally have a high recombination efficiency (>0.03). Figure 12 shows a comparison of the recombination efficiency of Inconel 617 (a nickel-chromium alloy), MA 956 (a mechanically alloyed iron-based dispersion-strengthened alloy), and coated and uncoated titanium aluminide alloy. The recombination efficiency for the coating is about one-fifth or less of that for uncoated alloys. These differences in recombination efficiency for titanium-aluminide alloy translate to temperature differences of about 100 K (see Fig. 9).

Concluding Remarks

A method for evaluating the recombination efficiency of thermal-control coatings for hypersonic vehicle applications has been demonstrated. The method uses the approach of Goulard for computing catalytic effects with the stagnation-point laminar-boundary-layer heat-transfer technique of Fay and Riddell. The method depends on a detailed energy balance for samples tested to define the catalytic interaction of surfaces with the hypersonic flowfield. Because the technique contains empirical adjustments to theoretical equations, the results are nominal and are primarily for use in the screening and development of coatings. They are most sensitive to uncertainties in experimental parameters for materials with low recombination efficiencies, which stresses the importance of including second-order heat-transfer terms when evaluating low-catalysis coatings.

The maximum uncertainty of recombination efficiency for low-catalysis samples is about 45% when the energy balance includes second-order heat-transfer terms. For a coating with a nominal recombination efficiency of 0.01, the bounds on recombination efficiency would be 0.006 and 0.015, which translates to temperature bounds of 1260 and 1310 K. Low-catalysis coatings have the potential to reduce the temperature of vehicles in hypersonic flight by 100 K for flight conditions with dissociated oxygen and nitrogen.

References

[1]Clark, R. K., Cunnington, G. R., and Robinson, J. C., "Vapor-Deposited Emittance-Catalysis Coatings for Superalloys in Heat Shield Applications," *Journal of Thermophysics and Heat Transfer*, Vol. 1, No. 1, 1987, pp. 28–34.

[2]Goulard, R., "On Catalytic Recombination Rates in Hypersonic Stagnation Heat Transfer," *Journal of Jet Propulsion*, Vol. 28, Nov. 1958, pp. 737–745.

[3]Pope, R. B., "Stagnation-Point Convective Heat Transfer in Frozen Boundary Layers," *AIAA Journal*, Vol. 6, No. 4, 1968, pp. 619–626.

[4]Scott, C. D., "Catalytic Recombination of Nitrogen and Oxygen on High Temperature Reusable Surface Insulation," AIAA Paper 80-1477, July 1980.

[5]Schaefer, J. W., Tong, H., Clark, K. J., Suchsland, K. E., and Neuner, G. J., "Analytic and Experimental Evaluation of Flowing Air Test Conditions

for Selected Metallics in a Shuttle TPS Application," NASA CR-2531, Aug. 1975.

[6]Anon., "E 422-83, Standard Method for Measuring Heat Flux Using a Water-Cooled Calorimeter," *1986 Annual Book of Standards, Part 15.03*, American Society for Testing Materials, 1986.

[7]Linnett, J. W., and Marsden, D. G. H., "The Kinetics of the Recombination of Oxygen Atoms at a Glass Surface," *Proceedings of the Royal Society of London, Series A: Mathematical and Physical Sciences*, Vol. 234, 1956, pp. 489–504.

[8]Dunkle, R. V., Edwards, D. K., Gier, J. T., Nelson, K. E., and Roddick, R. D., "Heated Cavity Reflectometer for Angular Reflectance Measurements," *Progress in International Research on Thermodynamic and Transport Properties*, edited by Joseph F. Masi and Donald H. Tsai, American Society of Mechanical Engineers, 1962, pp. 541–562.

[9]Touloukian, Y. S., and Dewitt, D. P., eds., *Thermal Radiative Properties Non-metallic Solids*, IFI/Plenum, New York, 1972, p. 18a.

[10]Jakob, M., *Heat Transfer*, Vol. I, Wiley, New York, 1949, pp. 51, 52.

[11]Cunnington, G. R., Funai, A. I., and Cassady, P. E., "Development of Techniques and Associated Instrumentation for High Temperature Emissivity Measurements," NASA CR-124423, June 1973.

[12]Cunnington, G. R., Clark, R. K., and Robinson, J. C., "Thermal Coatings for Titanium-Aluminum Alloys," NASA TM-107760, April 1993.

[13]Scala, S. M., "Hypersonic Heat Transfer to Surfaces Having Finite Catalytic Efficiency," General Electric Co., Aerophysics Research Memorandum No. 4, June 1957.

[14]Fay, J. A., and Riddell, F. R., "Theory of Stagnation Point Heat Transfer in Dissociated Air," *Journal of Aeronautical Sciences*, Vol. 25, No. 2, 1958, pp. 73–85.

[15]Zoby, E. V., and Sullivan, E. M., "Effects of Corner Radius on Stagnation-Point Velocity Gradients on Blunt Axisymmetric Bodies," NASA TM X-1067, March 1965.

[16]Zoby, E. V., "Empirical Stagnation-Point Heat-Transfer Relation in Several Gas Mixtures at High Enthalpy Levels," NASA TN D-4799, Oct. 1968.

[17]Stroud, C. W., and Brinkley, K. L., "Chemical Equilibrium of Ablation Materials Including Condensed Species," NASA TN D-5391, Aug. 1969.

[18]Pai, S., *Viscous Flow Theory, Vol. I—Laminar Flow*, Van Nostrand, Princeton, NJ, 1956, p. 10.

[19]Kolodziej, P., and Stewart, D. A., "Nitrogen Recombination on High-Temperature Reusable Surface Insulation and the Analysis of its Effect on Surface Catalysis," AIAA Paper 87-1637, June 1987.

[20]Willey, R. J., "Comparison of Kinetic Models for Atom Recombination on High-Temperature Reusable Surface Insulation," *Journal of Thermophysics and Heat Transfer*, Vol. 7, No. 1, 1993, pp. 55–62.